

XMM-NEWTON OBSERVATIONS OF THE VELA PULSAR

K. Mori¹, C.J. Hailey¹, F. Paerels¹ and S. Zane²

¹*Columbia Astrophysics Laboratory, 550 W 120th St., New York, NY 10027, USA*

²*MSSL, University College London, Holmbury St. Mary, Dorking, Surrey, RH5 6NT, UK*

ABSTRACT

We present spectral analysis from *XMM-Newton* observations of the Vela pulsar. We analyzed thermal emission from the pulsar dominating below ~ 1 keV since extracted spectra are heavily contaminated by nebular emission at higher energy. Featureless high-resolution spectra of the Reflection Grating Spectrometer aboard *XMM-Newton* suggest the presence of a hydrogen atmosphere, as previously indicated by *Chandra* results. Both the temperature and radius are consistent with those values deduced from *Chandra*. The derived *Chandra* and *XMM-Newton* temperature of $T^\infty \simeq (6.4\text{--}7.1) \times 10^5$ K at its age of $\sim 10^4$ years is below the standard cooling curve.

INTRODUCTION

The Vela pulsar is one of the best-studied pulsars in the radio band. It has an 89 millisecond period and the spin-down parameters indicate that the Vela pulsar is about 10^4 years old with magnetic field 3×10^{12} G. Nevertheless, multi-wavelength observations in the past two decades showed the Vela pulsar is a strong source at all wavelengths from the radio to the gamma-ray band. In the X-ray band, thermal emission was discovered by *ROSAT* (Ögelman et al., 1993). *ROSAT* observation also revealed a peculiar pulse profile with three peaks in the soft X-ray band. Non-thermal emission from its surrounding nebula is dominant at higher energies.

Recent *Chandra* observations revealed even more complex properties of the Vela pulsar and its nebula. With its high angular resolution, a *Chandra* image showed detailed structure in the surrounding nebula (Helfand et al., 2001; Pavlov et al., 2001b). No spectral features were found in the high energy resolution *Chandra* LETGS spectra of the resolved pulsar emission. No detection of spectral features excludes the presence of heavy element atmospheres on the surface (Pavlov et al., 2001a).

The Vela pulsar is also a strong source of non-thermal emission in the optical, X-ray and gamma-ray bands. The non-thermal component from the pulsar was resolved for the first time by *Chandra* (Pavlov et al., 2001a). Recent *RXTE* observations revealed complex timing properties associated with non-thermal emission from the pulsar, showing energy-dependent multiple peaks in folded lightcurves (Strickman et al., 1999; Harding et al., 2002). However, the origin of the peaks in the soft X-ray band, whether thermal or non-thermal, has yet to be determined.

The *XMM-Newton* observation of the Vela pulsar was performed with a 90 ksec exposure time on 1 Dec 2000. *XMM-Newton* is sensitive to faint sources such as isolated neutron stars due to its large effective area. Since the nebula turned out to be compact $\sim 10\text{--}20''$ (Helfand et al., 2001), the imaging capability of *XMM-Newton* cannot resolve the pulsar from the nebula. Therefore, the thermal component dominates at $E \lesssim 1$ keV and the nebula emission is dominant at $E \gtrsim 1$ keV in *XMM-Newton* spectra. We could not spatially resolve the non-thermal emission from the pulsar or study different components of the nebula. Instead, using the *XMM-Newton* data, we did the following: (1) a spectral fit to high sensitivity European Photon Imaging Camera (EPIC) (Strüder et al., 2001) data was used to determine thermal properties with high accuracy, (2) a search for spectral features in high resolution Reflection Grating Spectrometer (RGS) (den Herder et al., 2001) data was performed. All the data were processed by version 5.3.3 of the Scientific Analysis System (SAS) pipeline (Loiseau, 2003).

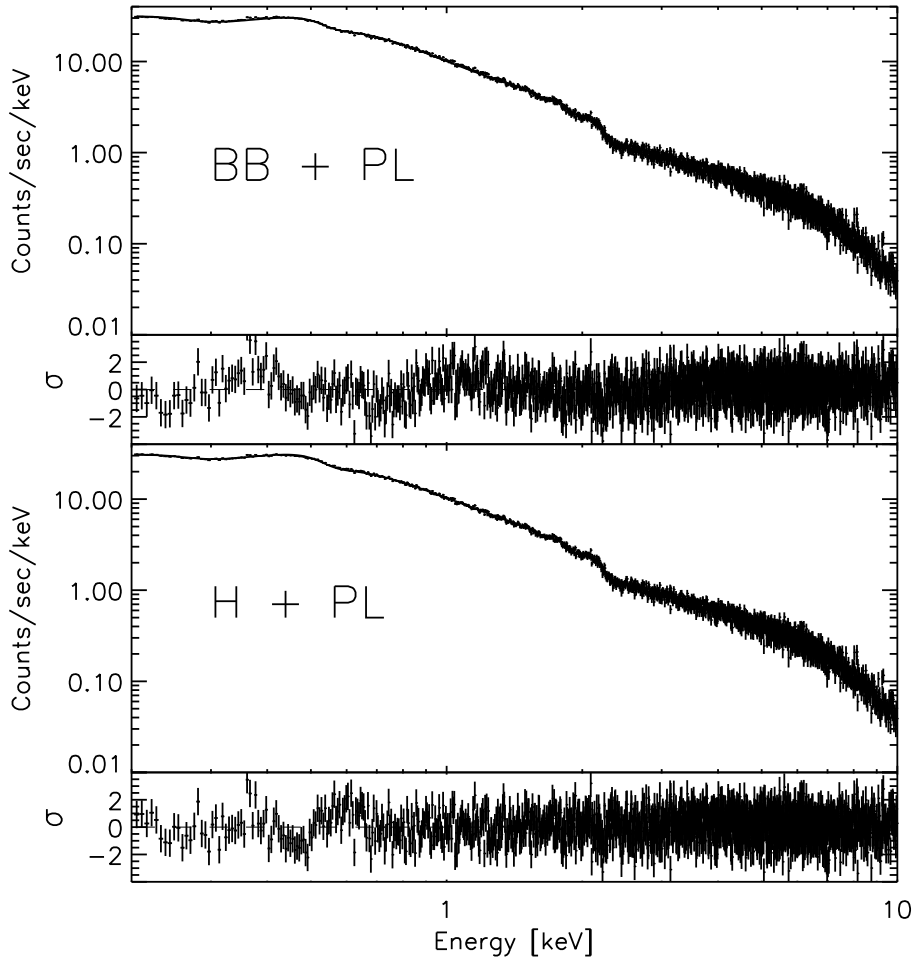


Fig. 1. *XMM-Newton*/EPIC-PN spectra fitted by Blackbody+Power-law (BB+PL) (top) and Hydrogen atmosphere+Power-law model (H+PL) (bottom). Residuals at ~ 0.5 keV are due to instrumental Oxygen edge.

EPIC PHASE-AVERAGED SPECTRAL ANALYSIS

We analyzed EPIC-PN data to determine the global features of the X-ray spectrum. Source data were extracted from a circular region with radius $r = 1'$ and events with CCD pattern 0 were selected. Such a source area includes more than 90% of the source counts at energies up to ~ 5 keV. However, the extracted spectra are heavily contaminated by nebular emission at $E \gtrsim 1$ keV. Unlike the recent *Chandra* results which resolved the pulsar emission from its nebula emission (Pavlov et al., 2001a), our analysis focuses on thermal emission from the pulsar at $E \lesssim 1$ keV. Systematic errors from nebular contamination are discussed later in this section. Background spectra were reduced from an annulus region between $r = 1'$ and $r = 2'$. Total EPIC-PN count rate from the $r < 1'$ region after subtracting background was 27.0 cts/sec.

We rebinned the data so that each spectral bin contained more than 25 counts. For the following spectral analysis, we used ready-made Response Matrix Files (RMFs) and Auxiliary Response Files (ARFs) generated by the SAS tool “arfgen”. For spectral fitting, we adopted a two-component model comprised of a thermal and non-thermal (power-law) spectrum. We applied two different thermal models to the data: a blackbody model (BB+PL model) and a magnetized hydrogen atmosphere model provided by V. Zavlin (Zavlin, 2003) at $B = 10^{12}$ G (H+PL model). When we fitted a hydrogen atmosphere model, we fixed the neutron star mass and radius to $1.4M_{\odot}$ and 10 km. Both thermal models fit the data well, yielding $\chi^2 \simeq 1.1$ (Figure 1 and Table 1). Figure 2 shows an N_H - T^{∞} contour plot with fixed power-law index and radius. Hydrogen atmospheres are in general harder than a blackbody since free-free absorption dominates in the X-ray band. Therefore, the temperature fitted by a magnetized hydrogen atmosphere model is lower than a blackbody fit (hence a larger radius for the hydrogen atmosphere fit).

The derived distance ($d = 256$ pc) is consistent with the distance from the parallax measurement ($d = 294_{-50}^{+76}$ pc).

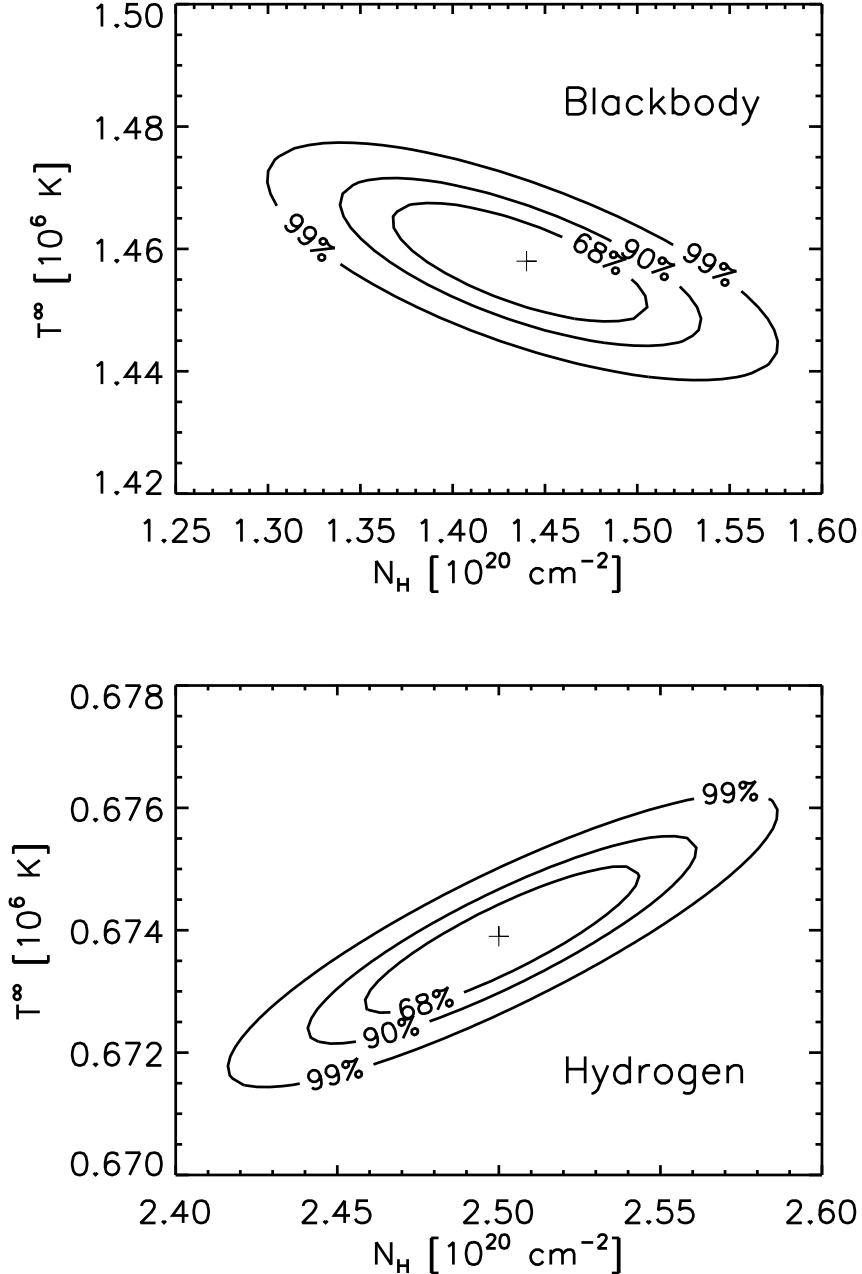


Fig. 2. Contour plot in N_H - T^∞ plane. Blackbody (top) and hydrogen atmosphere at $B = 10^{12}$ G (bottom).

pc) (Caraveo et al., 2001). For hydrogen atmosphere models, T^∞ and R^∞/d depend on other input parameters (e.g. M and R) weakly (Zavlin et al., 1998). The apparent radius corresponding to the measured distance is inferred to be $R^\infty/d_{294} = 15.0^{+6.5}_{-5.1}$ km where d_{294} is the distance in units of 294 pc.

We note that non-thermal spectra from the pulsar (obtained by *Chandra* observation) are about two orders of magnitude weaker than the nebular spectra, so the power-law component observed by *XMM-Newton* is dominated by the nebular contribution. The fitted power-law index ($\gamma \simeq 1.6$) probably represents a superposition of different nebular components, which were resolved by the *Chandra* observation (Pavlov et al., 2001b). The estimated luminosity of the power-law component in the EPIC-PN data is consistent with the *Chandra* result for the nebula ($L_{neb} = 8.3 \times 10^{32}$ ergs s^{-1} for $d = 294$ pc) (Pavlov et al., 2001b).

The derived parameters from both the blackbody and magnetized hydrogen atmosphere fit are in good agreement with the *Chandra* results. However, since the angular resolution of *XMM-Newton* is poorer than that of *Chandra*,

Table 1. Fitted parameters to *XMM-Newton* EPIC-PN spectra (pulsar plus nebula) in comparison with *Chandra* data (pulsar only).

Blackbody + Power-law		
	EPIC-PN	<i>Chandra</i>
N_H [10^{20} cm $^{-2}$]	$1.44^{+0.83}_{-0.85}$	2.2 ± 0.3
T^∞ [10^6 K]	$1.46^{+0.02}_{-0.02}$	1.50 ± 0.05
R^∞ [km] ^a	$2.50^{+0.15}_{-0.14}$	2.5 ± 0.2
L_{th}^∞ [10^{32} ergs s $^{-1}$] ^a	$2.02^{+0.34}_{-0.33}$	2.1 ± 0.3
γ ^b	$1.64^{+0.08}_{-0.08}$	2.7 ± 0.4
L_{pl} [10^{32} ergs s $^{-1}$] ^{a,b}	$8.56^{+0.11}_{-0.14}$	0.58 ± 0.08
χ^2_ν	1.16	1.1
Magnetized H atmosphere ^c + Power-law		
	EPIC-PN	<i>Chandra</i>
N_H [10^{20} cm $^{-2}$]	$2.50^{+0.16}_{-0.17}$	3.3 ± 0.3
T^∞ [10^6 K]	$0.674^{+0.034}_{-0.033}$	0.68 ± 0.03
d [pc]	256^{+44}_{-43}	210 ± 20
L_{th}^∞ [10^{32} ergs s $^{-1}$] ^a	$3.35^{+1.78}_{-1.77}$	5.2 ± 0.4
γ ^b	$1.59^{+0.12}_{-0.12}$	1.5 ± 0.3
L_{pl} [10^{32} ergs s $^{-1}$] ^{a,b}	$8.27^{+0.14}_{-0.14}$	0.21 ± 0.06
χ^2_ν	1.08	1.0

Errors for EPIC-PN data are 1 sigma level including both statistical and systematic uncertainty. For luminosity of non-thermal component in the range of 2–10 keV (L_{pl}), the error refers only to the statistical uncertainty since the smaller extracted region picks up less nebular emission.

^a We assumed the distance is 294 pc from the latest parallax measurement (Caraveo et al., 2001). We rescaled the *Chandra* results in Table 1 in Pavlov et al. (2001a) to $d = 294$ pc.

^b Note that these parameters are different from the *Chandra* results in comparison. However, the fitted parameters to the *XMM-Newton* data is dominated by the nebular component, while Pavlov et al. (2001a) extracted spectra from the pulsar.

^c We fixed the neutron star mass to $1.4M_\odot$ and the radius to 10 km for spectral fitting. Here $B = 10^{12}$ G.

our fitting parameters can be affected by systematic errors due the the nebular contamination. These errors are, in general, larger than the statistical ones. In order to estimate such errors, we examined the variations in the hydrogen atmosphere and blackbody parameters by using as extraction regions annuli of various radii; the errors reported in Table 1 reflect both statistical and systematic uncertainties. We can see that, when considering the effect on the nebular contamination, *Chandra* and *XMM-Newton* temperatures are in agreement at 1-sigma level.

SEARCH FOR SPECTRAL FEATURES IN RGS DATA

Reflection Grating Spectrometer data were taken in “spectroscopy” mode in order to take full advantage of the high spectral resolution. First, we extracted the 95% Point Spread Function (PSF) of the source region for both RGS 1 and 2 data. The background spectrum was reduced from outside the 98% PSF region. We generated responses by the SAS command “rgsrmfgen”. Total count rate was 1.0 cts/sec for both RGS 1 and 2 data. We extracted smaller regions of the source (50% and 70% PSF region) to maximize the number of thermal photons compared to nebular emission

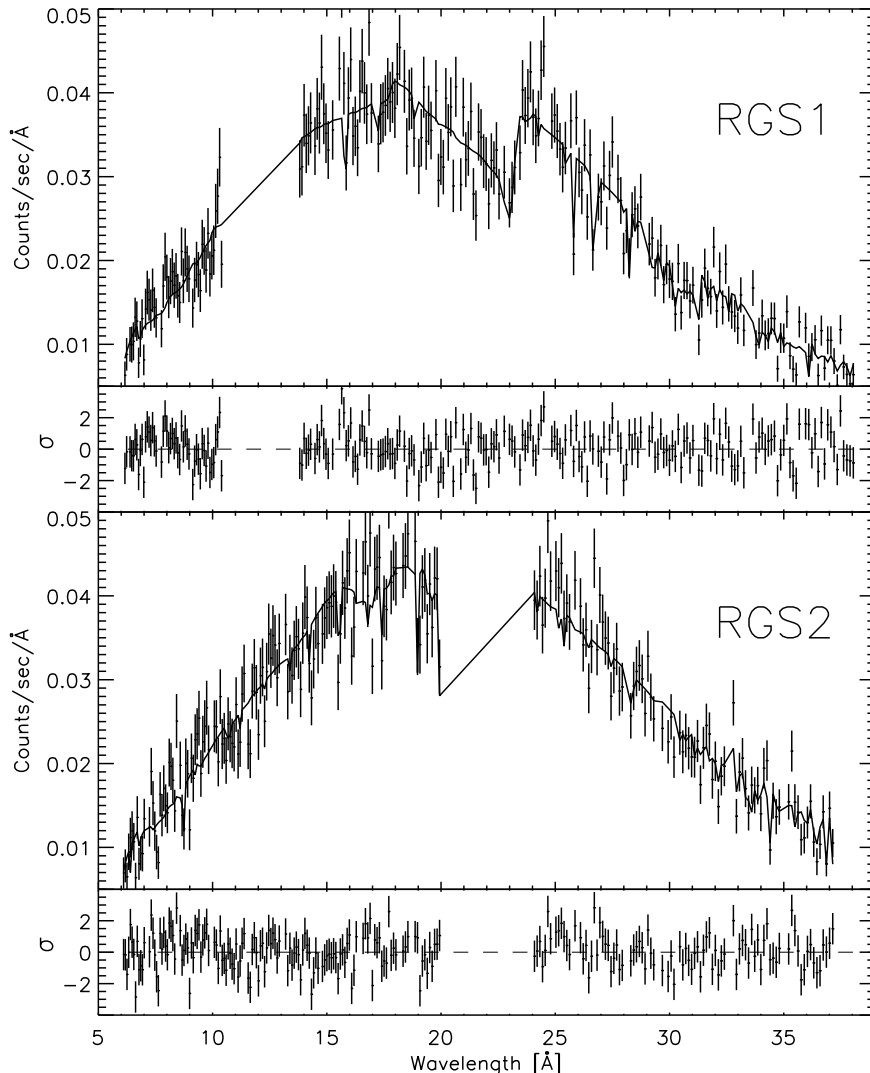


Fig. 3. *XMM-Newton*/RGS spectra fit by Hydrogen+Power-law model. The spectra were extracted from the 70% Point Spread Function (PSF) region.

photons. Figure 3 shows RGS spectra extracted from the 70% PSF region and fitted by the H+PL model. The data are plotted in the RGS bandpass ($\lambda = 6\text{--}38 \text{ \AA}$) after rebinning wavelength grids to $\lambda \sim 0.1 \text{ \AA}$.

The spectral fit by both the BB+PL and the H+PL model yield $\chi^2_{\nu} \simeq 1.2$ for both RGS 1 and 2 data. The fitted parameters were similar to the EPIC-PN results in Table 1. Several deviations from the continuum fit with less than 2 sigma significance are seen, but none of these wiggles were found in both RGS 1 and 2 data simultaneously. Therefore, we conclude that the RGS spectra are featureless.

SUMMARY

The results obtained with *XMM-Newton* for the Vela pulsar are in agreement with previous findings by *Chandra* (Pavlov et al., 2001a,b). The RGS data indicate that the thermal spectrum is featureless, and the EPIC-PN spectrum is well fitted by a magnetized hydrogen atmosphere model with $B = 10^{12} \text{ G}$. As it has been found with *Chandra*, with respect to a fit with the simple blackbody, the atmospheric model has the advantage that it gives a radius for the emitting region compatible with neutron star equations of state. Also, when *Chandra* data are fitted with an atmospheric model, the index of the power-law component above $\sim 1 \text{ keV}$ is remarkably consistent with that of the PL observed at optical and hard X-ray wavelengths. The power-law component observed with *XMM-Newton* is dominated by the nebular emission and the value of $L_{pl} \sim 8 \times 10^{32} \text{ erg s}^{-1}$ is again consistent with that observed by

Chandra (Pavlov et al., 2001b).

The presence of hydrogen is not surprising since a tiny amount of hydrogen constitutes an optically-thick layer in the atmosphere (Zavlin & Pavlov, 2002). Hydrogen could be accumulated on the surface by accretion or generated by spallation of fallback material (Bildsten et al., 1992). The derived large radius from the H+PL model implies that the thermal emission originates from the whole surface.

There is an important implication for the neutron star physics which is consistent with the *Chandra* and *XMM-Newton* results. Surface temperature for a given age reflects cooling processes via neutrino emission in the core. Recent studies show that neutron star cooling curves are dependent on various factors such as proton-to-neutron ratio, neutron star mass, magnetic field strength, neutron superfluidity and presence of exotic matter. Among various proposed models, a model which assumes normal composition (n , p and e) and the indirect URCA process was often quoted as the standard cooling model. The standard cooling model fits most cooling neutron stars, although recent X-ray observations found several neutron stars have surface temperatures below the standard cooling curve (Slane et al., 2002). For the Vela pulsar, the derived *Chandra* and *XMM-Newton* temperature of $T^\infty \simeq (6.4\text{--}7.1) \times 10^5$ K at its age $\sim 10^4$ years is below the standard cooling curve (Tsuruta et al., 2002).

ACKNOWLEDGEMENTS

We are grateful to V. Zavlin for providing us with the magnetized hydrogen atmosphere model.

REFERENCES

- Bildsten, L. and Salpeter, E. E. & Wasserman, I., The fate of accreted CNO elements in neutron star atmospheres - X-ray bursts and gamma-ray lines, *Astrophys. J.*, **384**, 143-176, 1992.
- Caraveo, P. A., De Luca, A., Mignani, R. P. et al., The distance to the Vela pulsar gauged with Hubble Space Telescope parallax observations, *Astrophys. J.*, **561**, 930-937, 2001.
- den Herder, J. W., Brinkman, A. C., Kahn, S. M. et al, The Reflection Grating Spectrometer on board XMM-Newton, *Astron. Astrophys.*, 365, L7-L17, 2001.
- Harding, A. K., Strickman, M. S., Gwinn, C. et al., The multicomponent nature of the Vela pulsar non-thermal X-Ray spectrum, *Astrophys. J.*, **576**, 376-380, 2002.
- Helfand, D. J., Gotthelf, E. V., & Halpern, J. P., Vela pulsar and its synchrotron nebula, *Astrophys. J.*, **556**, 380-391, 2001.
- Loiseau, N., Users' Guide to the XMM-Newton Science Analysis System, http://xmm.vilspa.esa.es/external/xmm_user_support/documentation/index.shtml, 2003.
- Ögelman, H., Finley, J. P., & Zimmerman, H. U., Pulsed X-rays from the Vela pulsar, *Nature*, **361**, 136-138, 1993.
- Pavlov, G. G., Zavlin, V. E., Sanwal, D. et al., The X-ray spectrum of the Vela pulsar resolved with Chandra, *Astrophys. J.*, **552**, L129-L133, 2001a.
- Pavlov, G. G., Kargaltsev, O. Y., Sanwal, D. et al., Variability of the Vela pulsar wind nebula observed with Chandra, *Astrophys. J.*, **554**, L189-L192, 2001b.
- Slane, P. O., Helfand, D. J., & Murray, S. S., New constraints on neutron star cooling from Chandra observations of 3C 58 *Astrophys. J.*, **571**, L45-L49, 2002.
- Strickman, M. S., Harding, A. K., & de Jager, O. C., A Rossi X-Ray timing explorer observation of the Vela pulsar: filling in the X-Ray gap, *Astrophys. J.*, **524**, 373-378, 1999.
- Strüder, L., Briel, U., Dennerl, K. et al., The European Photon Imaging Camera on XMM-Newton: The pn-CCD camera *Astron. Astrophys.*, L18-L26, 2001.
- Tsuruta, S., Teter, M. A., Takatsuka, T. et al., Confronting neutron star cooling theories with new observations, *Astrophys. J.*, **571**, L143-L146, 2002.
- Zavlin, V. E., Pavlov, G. G., & Trumper, J., The neutron star in the supernova remnant PKS 1209-52, *Astron. Astrophys.*, 331, 821-828, 1998.
- Zavlin, V. E. & Pavlov, G. G., Modeling neutron star atmospheres, *proceedings of the 270. WE-Heraeus Seminar on Neutron Stars, Pulsars and Supernova Remnants*, MPE-Report 278 (astro-ph/0206025), 263-272, 2002.
- Zavlin, V. E., private communication, 2003.